2D Aluminum Monoxide Nanosheets: A Computational Study

Shiru Lin,[1] Yanchao Wang,[2] Zhongfang Chen[1,*]

[1] Department of Chemistry, University of Puerto Rico, Rio Piedras Campus, San Juan, PR 00931, USA

[2] State Key Lab of Superhard Materials, Jilin University, Changchun 130012, China

To whom correspondence should be addressed. Email: zhongfangchen@gmail.com (ZC)

Abstract

By means of density functional theory (DFT) computations and Particle Swarm Optimization (PSO) structure searches, we herein predict five low-lying energy structures of two-dimensional (2D) aluminum monoxide (AlO) nanosheets. Their high cohesive energies, absence of imaginary phonon dispersions, and good thermal stabilities make them feasible targets for experimental realizations. These monolayers exhibit diverse structural topologies, for instance, *PmA*- and *Pmm*-AlO possess buckled four- and six-membered AlO rings, while *P62*-, *PmB*-, *P6m*-AlO have pores of varied sizes. Interestingly, the energetically most preferred monolayers, *PmA*- and *Pmm*-AlO, feature wide band gaps (2.45 and 5.13 eV, respectively), which are promising for green and blue light emitting devices (LEDs) and photodetectors.

Keywords: 2D materials, density functional calculations, particle swarm optimization, wide band gap semiconductor

TOC

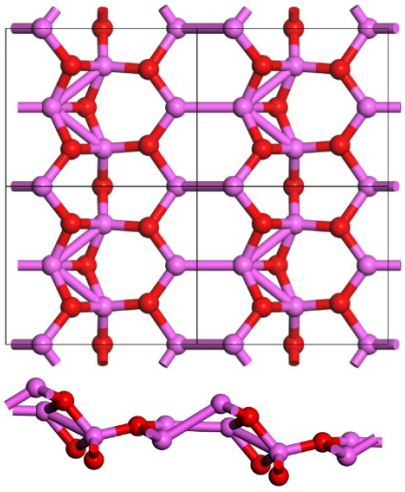

1. Introduction

The successful experimental realization of graphene [1] and the discovery of its exceptional electronic and transport properties [2-6] inspired tremendous efforts to investigate other two-dimensional (2D) materials [7-14]. So far, numerous elemental 2D materials, such as group IV silicene [15-21], germanene [22-27], and stanine [28-32], group V phosphorene [33-39], arsenene [40-43] and antimonene [41-47] have been experimentally fabricated and/or theoretically studied. Aluminene, as an important member of group III monolayers, has also been explored theoretically, and the buckled aluminene (*P*-3m1 point group) was reported to be the lowest energy and of metallic nature [48, 49].

Aluminum can be easily oxidized, and aluminum oxides have been commonly utilized in different areas. There are three aluminum oxide compounds: aluminum monoxide (AlO), dialuminum oxide (Al_2O), and dialuminum trioxide (Al_2O_3). Both AlO and Al_2O are of gas state [50, 51] with linear structure [52, 53]. The most known aluminum oxide is Al_2O_3, which is widely used as solid electrolytes [54] and catalysts [55]. Aluminum and oxygen are two of the most abundant elements in the earth, however, scarce work has focused on 2D aluminum oxide materials. Recently, Song *et al.* [56] theoretically designed a planar Al_2O_3 layered material with a direct band gap of 5.99 eV. In its honeycomb lattice, aluminum atoms are at vertexes of hexagons and linearly connected by oxygen atoms. Apparently, different oxygen concentrations in aluminum oxides can lead to various stable 2D nanostructures, and these nanosheets may present rather unique properties. Thus, it is interesting to explore

geometric structures and electronic properties of 2D aluminum oxide nanosheets with other stoichiometries.

In this work, by means of density functional theory (DFT) computations and global minimum structure searches, we theoretically predicted the five low-lying-energy 2D aluminum monoxide (AlO) nanosheets. These newly predicted monolayers have varied structural topologies and cover a wide range of band gaps (from 1.76 to 6.51 eV). Their highly positive cohesive energies, absence of imaginary phonon dispersion and good thermal stability indicate the feasibility of their experimental realizations. Especially, the two lowest energy configurations, *PmA*- and *Pmm*-AlO, which feature wide band gaps (2.45 and 5.13 eV, respectively), are promising for many applications, which are highly recommended as experimental targets.

2. Computation Methods

Our DFT computations were performed using ultrasoft pseudopotentials as implemented in the CASTEP code [57]. The suitability of ultrasoft pseudopotential for the systems under study was validated (Fig. S1 and 2, S-Table 1). The electron exchange-correlation functional was treated using generalized gradient approximation (GGA) in the form proposed by Perdew, Burke and Ernzerhof (PBE). The energy cutoff was set to 500 eV, the convergence tolerance was 10^{-5} eV, and the vacuum spaces are more than 15 Å, so that the interactions between adjacent layers can be ignored. The Monkhost-Pack *k* points were set as 7×3×1, 5×6×1, 4×4×1, 2×6×1, 4×4×1, respectively, for geometry optimizations and self-consistent calculations of the

five monolayers under investigation. We carried out both spin-polarized and spin-unpolarized computations and ensured that all these AlO monolayers have no magnetism. To evaluate the dynamic stability of AlO monolayers, we computed the phonon dispersions using 2×2×1 supercells and 10^{-6} eV convergence tolerances.

We also performed *Ab initio* molecular dynamics (AIMD) simulations using a Nosé-Hoover thermostat in NVT canonical ensemble to evaluate the thermal stability of AlO monolayers. The 2×2×1 AlO supercells (3×2×1 supercell for *Pmm*-AlO) were simulated at different temperature of 300, 500 and 1000 K, and each simulation lasted for 10 *ps* with a time step of 2.0 *fs*.

Since PBE functional tends to underestimate the band gap values, while recent studies demonstrated that the GLLB-sc potential as implemented in GPAW code [58] empowers improved band gap calculations by including derivative discontinuity absent in PBE [59-61], we also carried out the band gap computations by GLLB-sc potential to get more accurate band gaps.

The particle-swarm optimization (PSO) method as implemented in CALYPSO code [62] was used to search for stable 2D AlO monolayers. The optimizations were performed by CASTEP code using PBE functional. In our calculations, the population size was set to 30, and the number of generation was set to 50. Unit cells containing 1 to 6 aluminum atoms and the same numbers of oxygen atoms were considered. The CALYPSO search helped us to find the low-lying energy structures of AlO monolayers in the 2D space.

3. Results and discussion

3.1 Geometric Structures

Our CALYPSO search resulted in five low-lying energy 2D aluminum oxide nanosheets (Figure 1), which are denoted by the first three letters/numbers of their symmetries, i.e. *PmA*-, *Pmm*-, *P62*-, *PmB*- and *P6m*- AlO (two structures with *Pm* symmertry are differentiated by A and B). These monolayers exhibit diverse structural topologies, as indicated by their key structural parameters (Table 1) and optimized geometries (Figure 1), and can be divided into two groups: the buckled *PmA*- and *Pmm*-AlO, and the planar and porous *P62*-, *PmB*- and *P6m*-AlO monolayers.

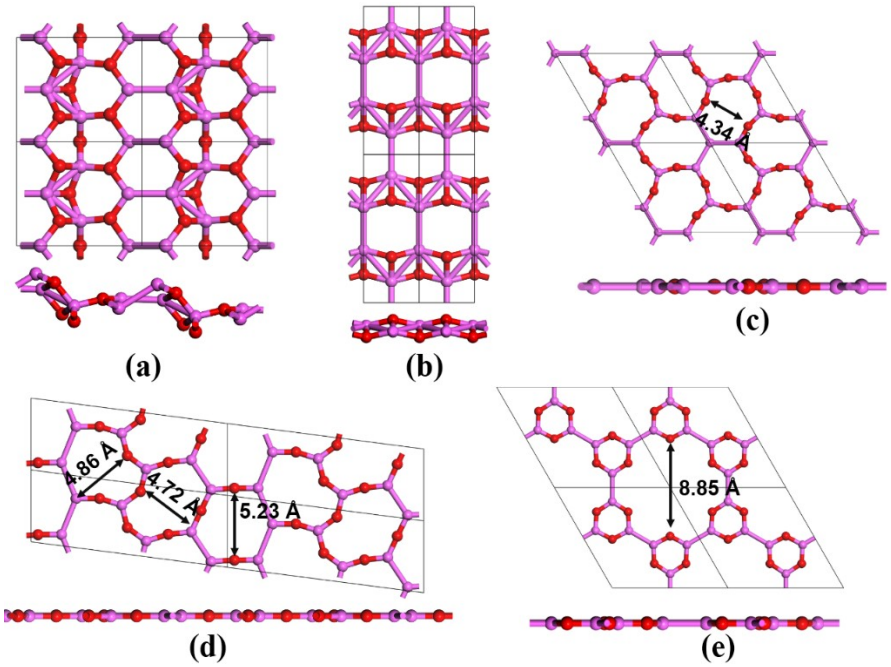

Figure 1. Top and side views of (a) *PmA*-, (b) *Pmm*-, (c) *P62*-, (d) *PmB*- and (e) *P6m*-AlO monolayers. The red and rose-carmine atoms represent O and Al atoms, respectively. For clarity, (2 × 2 × 1) supercells are presented here.

Both buckled monolayers, *PmA*- and *Pmm*-AlO, consist of six- and

four-membered rings. What they differ most is that only *PmA*-AlO has lines of AlO-interlaced six-membered Al_3O_3 rings, leading to their different buckled structures with the thinness (h) of 0.152 and 0.076 Å, respectively. In comparison, the remaining three AlO monolayers are planar, among which *P62* and *PmB* have 10- and 10/11/9-membered rings with the pore size of 4.34 and 4.86/4.72/5.23 Å, respectively, and *P6m* possesses quite big 18-membering rings with a pore size of 8.85 Å in diameter.

Table 1. Key structural parameters (lattice parameters, Al-O and Al-Al bond lengths), cohesive energies (E_b, eV/atom), and band gaps (E_g, eV) of AlO monolayers

Structure	*PmA*-AlO	*Pmm*-AlO	*P62*-AlO	*PmB*-AlO	*P6m*-AlO
Symmetry	*Pm*	*Pmmn*	*P-62m*	*Pm*	*P6/mmm*
Lattice parameters (Å)	*a*=7.25; *b*=6.00	*a*=3.62; *b*=9.67	*a*=*b*=9.12	*a*=14.42; *b*=5.23	a=b=10.55
Al-O (Å)	1.70~1.94	1.77; 1.91	1.68	1.68; 1.69	1.72
Al-Al (Å)	2.55~2.72	2.79; 2.76	2.54	2.60	2.56
E_b	5.61	5.55	5.39	5.37	5.36
E_g (PBE)	0.81	2.42	1.56	0.28	3.53
$\underline{E}_g$ (GLLB-sc)	2.45	5.13	3.54	1.76	6.51

A significant difference between the above mentioned two groups is that the buckled structures (*PmA*-AlO and *Pmm*-AlO) contain tetra-, penta-, and hexa-coordinated aluminum atoms as well as tri-coordinated oxygen atoms, while the planar porous ones (*P62*-, *PmB*- and *P6m*-AlO) merely contain tri-coordinated aluminum atoms and bi-coordinated oxygen atoms (Fig. 1). Thus, it is the larger coordinate numbers, more chemical bonds, that makes *PmA*- and *Pmm*-AlO

monolayers energetically more favorable than other configurations.

3.2. Thermodynamic, Dynamic and thermal Stabilities

The stability of a material is highly important for its experimental realizations and future applications. Thus, we carefully examined the thermodynamic, dynamic and thermal stabilities of these AlO monolayers.

First, we examined their thermodynamic stabilities by computing their cohesive energies (E_b) defined as

$$E_c = nE_{Al} + nE_O - E_{AlO} / 2n$$

Where n stands for number of aluminum/oxygen atoms in an unitcell (*Pmm*-AlO unitcell is composed of four aluminum atoms and four oxygen atoms, while the others contain six aluminum atoms and six oxygen atoms); E_{Al}, E_O and E_{AlO} are the total energies of the single atoms and the material unit cell. According to our definition, the structure with a more positive cohesive energy (lower system energy) is thermodynamically more favorable. The computed cohesive energies of these newly predicted AlO monolayers are all highly positive, which are 5.61, 5.55, 5.39, 5.37, 5.36 eV/atom, respectively (Table 1). These cohesive energies are smaller than that of 2D-Al_2O_3 (5.97 eV/atom [56]), but higher than the buckled-aluminene (3.18 eV/atom) at the same theoretical level, indicating the importance of strong Al-O covalent bonds for the stability of aluminum oxides. Note that *PmA*-AlO has the highest average cohesive energy (5.61 eV/atom), followed by *Pmm*-AlO, the other buckled nanosheets, which is 0.06 ev/atom higher in system energy. However, the three planar and porous structures are 0.22-0.25 eV/atom higher in system energies. Thus, *PmA*-AlO is the

global minimum structure in the 2D space, and has a better chance for experimental realization, while others are metastable but also highly feasible experimentally.

Secondly, we investigated the dynamic stabilities of these AlO monolayers by computing their phonon dispersions. Note that, no significant imaginary frequency was found. Thus, the phonon dispersions confirm that these five 2D AlO nanosheets are dynamically stable and local minima.

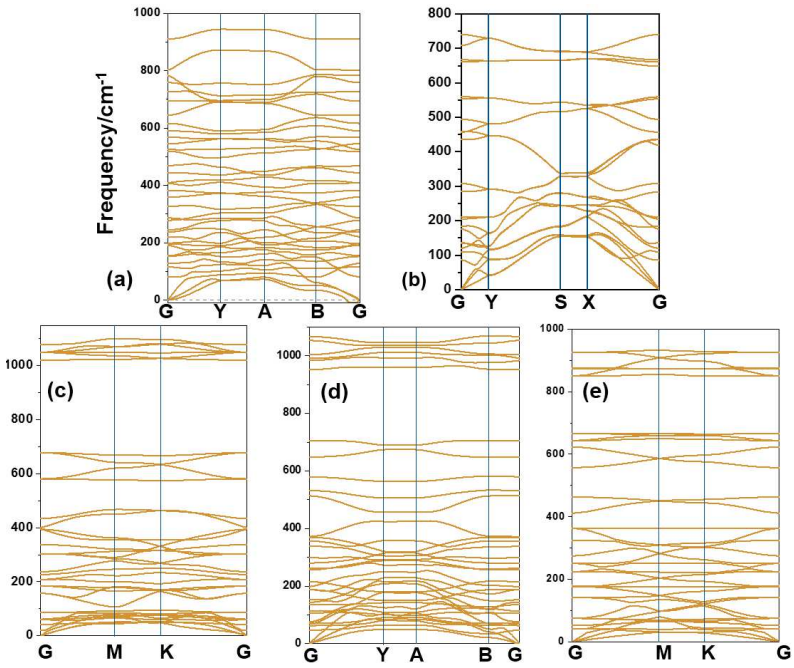

Figure 2. Phonon dispersions of (a) *PmA*-, (b) *Pmm*-, (c) *P62*-, (d) *PmB*-, and (e) *P6m*-AlO monolayers.

Thirdly, we evaluated the thermal stability of aluminum monoxide nanosheets by AIMD simulations (Figure 3). At room temperature (300K), all the five AlO monolayers well maintain their geometries; *Pmm-, P62-* and *P6m*-AlO nanosheets can preserve their structures at temperatures up to 1000 K, indicating their outstanding stabilities at extremely high temperatures.

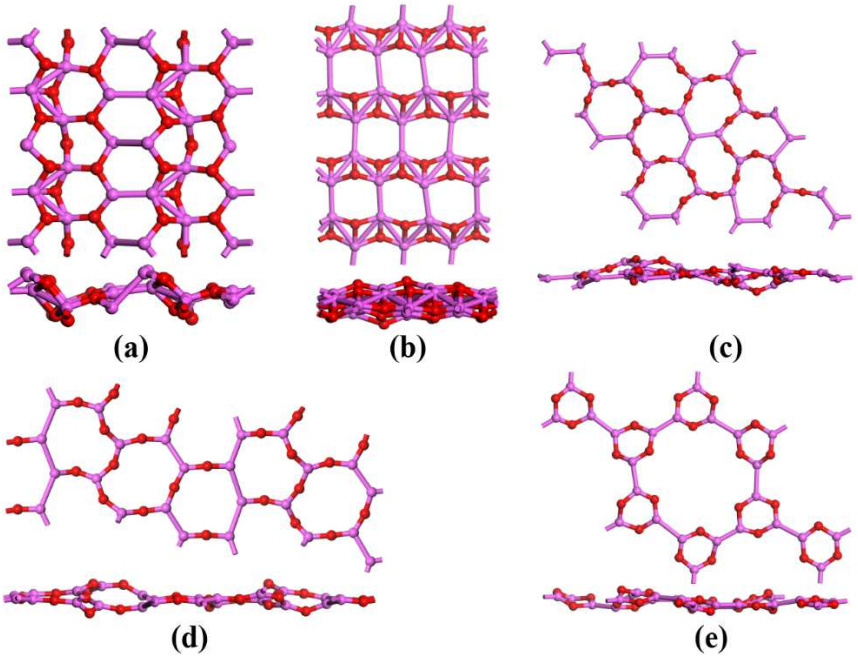

Figure 3. Snapshots of (a) *PmA*-, (b) *Pmm*-, (c) *P62*-, (d) *PmB*-, and (e) *P6m*-AlO equilibrium structures at (a) 300 K, (b) 1000 K, (c) 1000 K, (d) 300 K and (e) 1000 K at the end of 10 *ps* AIMD simulations.

In general, the good thermodynamic, dynamic and thermal stabilities, as revealed by the computed binding energies, phonon dispersions, AIMD simulations, and PSO global minimum search, strongly indicate the high feasibility for the experimental realization of these predicted aluminum monoxide nanosheets.

3.3. Electronic properties

To study the electronic properties of 2D AlO monolayers, we first computed their band structures as well as partial density of states (PDOS) at PBE level of theory (Figure 4). No band line across the Fermi level is available in all the computed band structures, thus all these five AlO monolayers are semiconducting. Nevertheless, these AlOs monolayers possess diverse band gap types and band gap values (table 1).

Pmm-AlO, *P62*-AlO and *PmB*-AlO have direct band gaps at G point, and their band gaps are 2.42, 1.56 and 0.28 eV at PBE level, respectively, at PBE level of theory; While *PmA*-AlO and *P6m*-AlO have indirect band gaps of 0.81 and 3.53 eV, respectively, by PBE functional. The conduction band minimum (CBM) of *PmA*-AlO is at A point (0.5, 0.5, 0), and valence band maximum (VBM) is at Y point (0, 0.5, 0); while the CBM of *P6m*-AlO is at K point (0.333, 0.333, 0), and VBM is at G point.

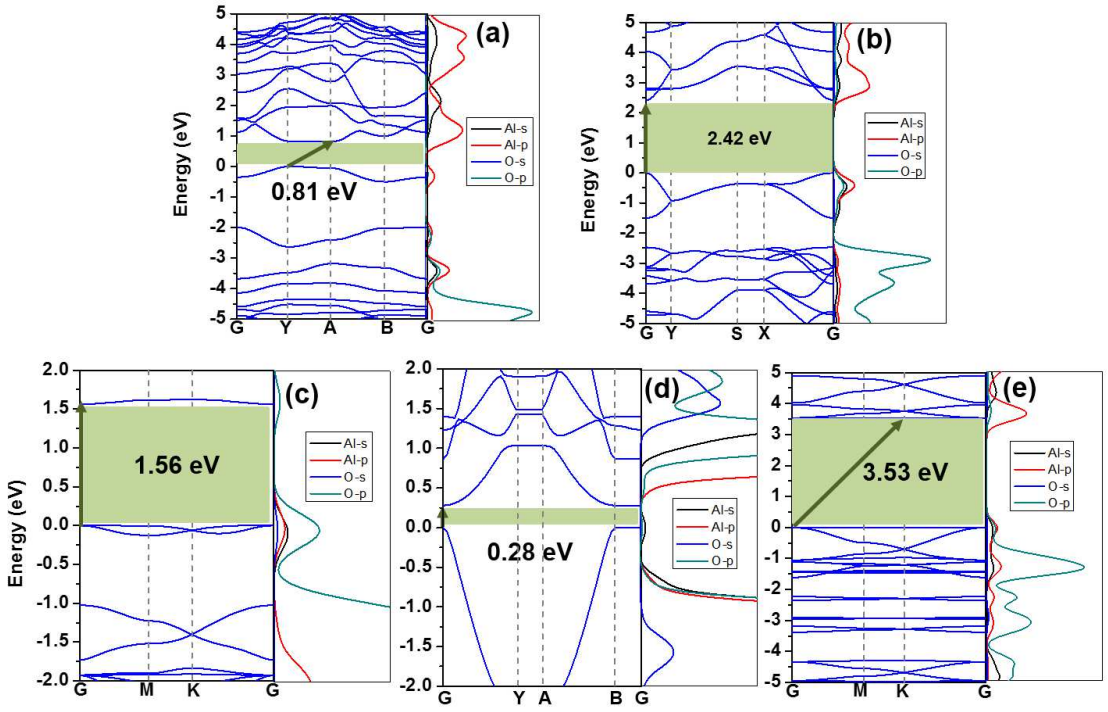

Figure 4. Band structures of (a) *PmA*-, (b) *Pmm*-, (c) *P62*-, (d) *PmB*- and (e) *P6m*-AlO monolayers (by PBE functional).

Then, we carefully analyzed the PDOS plots to check the orbital contributions to the bands close to the Fermi level. For the lowest-energy AlO monolayer, i.e., *PmA*-AlO, its VBM and CBM are mainly donated by *p* orbitals of aluminum atoms, and their electron densities are mostly contributed by *p* orbital of aluminum atoms

along Al_4O_2 rings (Figure 5a and 5b). The VBM of *Pmm*-AlO, the second lowest-energy AlO monolayer, is contributed by the hybridization of *p* orbitals of oxygen and *s* and *p* orbitals of aluminum atoms, and its CBM mainly comes from *p* orbitals of aluminum atoms (Figure 5c and 5d).

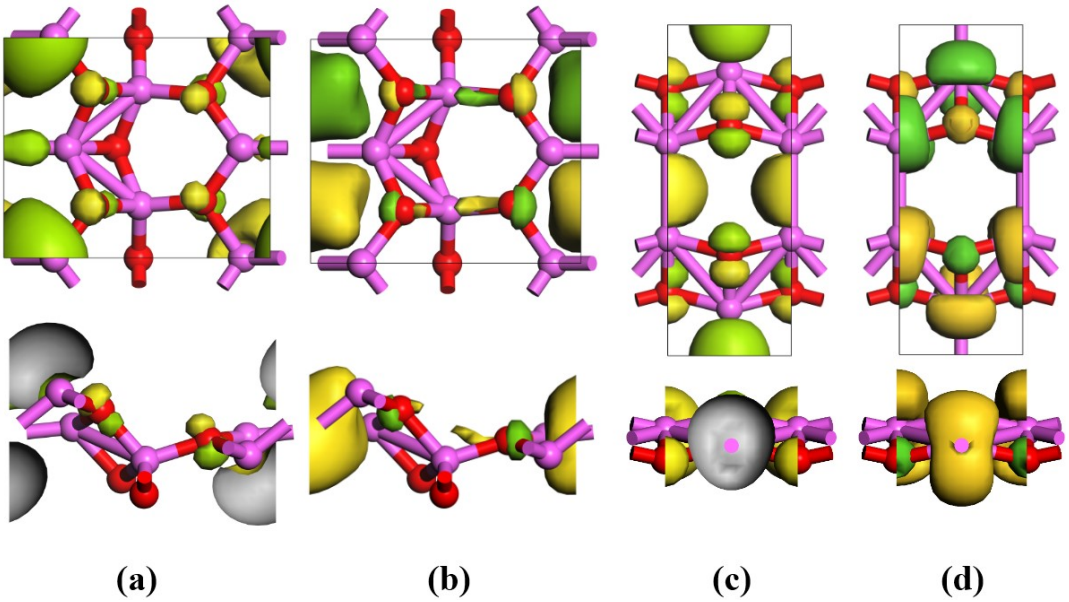

Figure 5. Electron density distributions (isosurface = 0.04 a.u.): (a) VBM and (b) CBM of *PmA*-AlO monolayer; (c) VBM and (d) CBM of *Pmm*-AlO monolayer.

We also computed the band gap using GLLB-sc functional, whose good performance to predict band gap values was well validated [59]. The band gap of *PmA*-, *Pmm*, *P62*-, *PmB*- and *P6m*- AlO monolayers are 2.45, 5.13, 3.54, 1.76 and 6.51 eV, respectively, covering a wide range of band gaps.

Interestingly, the two lowest energy AlO monoalyers, which are expected to be dominant experimentally due to their much better thermodynamic stabilities, both feature wide band gaps larger than 2.0 eV. [41, 63-65] Note that wide band gap

semiconductors are essential to realize devices for high-voltage [66], high-power and high-temperature operations [67, 68], but have not well developed due to the scarcity of such materials. Similar to h-BN [69, 70], our newly predicted, experimentally feasible 2D *Pmm*- and *PmA*-AlO monolayers are wide band gap semiconductors, thus are very promising for applications, among others, for high-power ultra-thin electronics, green and blue (LEDs), blue-violet laser diodes and photodetectors [71-73].

4. Conclusion

We theoretically investigated the structure, stability and electronic properties of five low-lying energy 2D aluminum monoxide nanosheets by means of PSO searches and systematic DFT computations. Among the five structures under investigation, the buckled *PmA*-AlO is of the lowest energy, which is closely followed by the buckled structure, *P*mm-AlO, while other three structures, namely *P62*-, *PmB*- and *P6m*, are planar and have pores with different sizes (4.34-8.85 Å diameters). These monolayers are semiconducting with indirect or direct band gaps ranging from 1.76 to 6.51 eV (GLLB-sc functional). All these monolayers are thermodynamically, dynamically and thermally stable, as indicated by their rather high cohesive energies, absence of imaginary phonon dispersions, and well preserved geometric structures in high temperatures, which strongly indicate the feasibility for their experimental realizations. In particular, the two lowest energy AlO monolayers, which are expected to be prepared with larger chances, are both wide band gap semiconductors, which endow them enormous potentials in devices such as high-power ultra-thin electronics, green

and blue LEDs, blue-violet laser diodes and photodetectors. We hope that our newly predicted 2D AlO nanosheets will inspire more efforts on 2D main group oxide materials with unusual structural and electronic properties.

Acknowledgement

This work is supported by NSF-CREST Center for Innovation, Research and Education in Environmental Nanotechnology (CIRE2N) (Grant Number HRD-1736093) and NASA (Grant 17-EPSCoRProp-0032).

Electronic Supplementary Information

Optimized geometric structure and predicted band structure of *PmA*-AlO and *Pmm*-AlO nanosheets using norm-conserving pseudopotential at PBE level of theory, and the comparison of the computational results using norm-conserving pseudopotential and ultrasoft pseudopotential. This material is available free of charge via the Internet at http://journal.hep.com.cn

Reference

1. K. S. Novoselov, A. K. Geim, S. V. Morozov, D. Jiang, Y. Zhang, S. V. Dubonos, I. V. Grigorieva and A. A. Firsov, Electric Field Effect in Atomically Thin Carbon Films, *Science*, 306(5696), 666(2004).

2. Y. Zhang, Y.-W. Tan, H. L. Stormer and P. Kim, Experimental observation of the quantum Hall effect and Berry's phase in graphene, *Nature*, 438(7065), 201(2005).

3. C. L. Kane and E. J. Mele, Quantum spin Hall effect in graphene, *Phys. Rev. Lett.*, 95(22), 226801(2005).

4. K. S. Novoselov, A. K. Geim, S. Morozov, D. Jiang, M. Katsnelson, I. Grigorieva, S. Dubonos and A. Firsov, Two-dimensional gas of massless Dirac fermions in graphene, *Nature*, 438(7065), 197(2005).

5. S. V. Morozov, K. S. Novoselov, M. I. Katsnelson, F. Schedin, D. C. Elias, J. A. Jaszczak and A. K. Geim, Giant Intrinsic Carrier Mobilities in Graphene and Its Bilayer, *Phys. Rev. Lett.*, 100(1), 016602(2008).

6. F. Schwierz, Graphene transistors, *Nat. Nanotech.*, 5(7), 487(2010).

7. A. Molle, J. Goldberger, M. Houssa, Y. Xu, S. C. Zhang and D. Akinwande, Buckled Two-Dimensional Xene Sheets, *Nat. Mater.*, 16(2), 163(2017).

8. Q. Tang and Z. Zhou, Graphene-Analogous Low-Dimensional Materials, *Prog. Mater. Sci.*, 58(8), 1244(2013).

9. K. S. Novoselov, A. Mishchenko, A. Carvalho and A. H. Castro Neto, 2d Materials and Van Der Waals Heterostructures, *Science*, 353(6298), aac9439(2016).

10. S. Lin, J. Gu, Y. Wang, Y. Wang, S. Zhang, X. Liu, H. Zeng and Z. Chen, Porous Silaphosphorene, Silaarsenene and Silaantimonene: a Sweet Marriage of Si and P/As/Sb., *J. Mater. Chem. A*, 6(8), 3738(2018).

11. G. Wang, R. Pandey and S. P. Karna, Atomically thin group V elemental films: theoretical investigations of antimonene allotropes, *ACS Appl. Mater. & Interfaces*, 7(21), 11490-11496(2015).

12. L. Kou, C. Chen and S. C. Smith, Phosphorene: Fabrication, Properties, and Applications, *J. Phys. Chem. Lett.*, 6(14), 2794-2805(2015).

13. S. Z. Butler, S. M. Hollen, L. Cao, Y. Cui, J. A. Gupta, H. R. Gutierrez, T. F. Heinz, S. S. Hong, J. Huang, A. F. Ismach, E. Johnston-Halperin, M. Kuno, V. V. Plashnitsa, R. D. Robinson, R. S. Ruoff, S. Salahuddin, J. Shan, L. Shi, M. G. Spencer, M. Terrones, W. Windl and J. E. Goldberger, Progress, Challenges, and Opportunities in Two-Dimensional Materials Beyond Graphene, *ACS Nano*, 7(4), 2898(2013).

14. Q. Tang, Z. Zhou, Z. Chen, *Wiley Interdiscip. Rev.: Comput. Mol. Sci.*, 5(5), 360(2015).

15. J. J. Zhao, H. S. Liu, Z. M. Yu, R. G. Quhe, S. Zhou, Y. Y. Wang, C. C. Liu, H. X. Zhong, N. N. Han, J. Lu, Y. G. Yao and K. H. Wu, Rise of Silicene: A Competitive 2d Material, *Prog. Mater. Sci.*, 83, 24(2016).

16. G. G. Guzmán-Verri and L. C. Lew Yan Voon, Electronic Structure of Silicon-Based Nanostructures, *Phys. Rev. B*, 76(7), 075131(2007).

17. L. Chen, C. C. Liu, B. Feng, X. He, P. Cheng, Z. Ding, S. Meng, Y. Yao and K. Wu, Evidence for Dirac Fermions in a Honeycomb Lattice Based on Silicon, *Phys. Rev. Lett.*, 109(5), 056804(2012).

18. P. De Padova, P. Vogt, A. Resta, J. Avila, I. Razado-Colambo, C. Quaresima, C. Ottaviani, B. Olivieri, T. Bruhn and T. Hirahara, Evidence for Dirac fermions in a honeycomb lattice based on silicon, *Appl. Phys. Lett.*, 102(16), 163106(2013).

19. E. Durgun, S. Tongay and S. Ciraci, Silicon and III-V compound nanotubes: Structural and electronic properties, *Phys. Rev. B*, 72(7), 075420 (2005).

20. U. Rothlisberger, W. Andreoni and M. Parrinello, Structure of nanoscale silicon clusters, *Phys. Rev. Lett.*, 72(5), 665(1994).

21. P. Vogt, P. De Padova, C. Quaresima, J. Avila, E. Frantzeskakis, M. C. Asensio, A. Resta, B. Ealet and G. Le Lay, Silicene: compelling experimental evidence for graphenelike two-dimensional silicon, *Phys. Rev. Lett.*, 108(15), 155501(2012).

22. S. Cahangirov, M. Topsakal, E. Akturk, H. Sahin and S. Ciraci, Two- and one-dimensional honeycomb structures of silicon and germanium, *Phys. Rev. Lett.*, 102(23), 236804(2009).

23. K. Takeda and K. Shiraishi, Theoretical possibility of stage corrugation in Si and Ge analogs of graphite, *Phys. Rev. B, Condensed matter*, 50(20), 14916(1994).

24. Y. Jing, Z. Zhou, C. R. Cabrera and Z. F. Chen, Graphene, inorganic graphene analogs and their composites for lithium ion batteries, *J. Mater. Chem. A*, 2(31), 12104(2014).

25. M. Dávila, L. Xian, S. Cahangirov, A. Rubio and G. Le Lay, Germanene: a novel two-dimensional germanium allotrope akin to graphene and silicene, *New J. Phys.*, 16(9), 095002(2014).

26. M. Houssa, E. Scalise, K. Sankaran, G. Pourtois, V. V. Afanas'ev and A. Stesmans, Electronic properties of hydrogenated silicene and germanene, *Appl.*

Phys. Lett., 98(22), 223107(2011).

27. L. Li, S. Z. Lu, J. Pan, Z. Qin, Y. Q. Wang, Y. Wang, G. Y. Cao, S. Du and H. J. Gao, Buckled Germanene Formation on Pt(111), *Adv. Mater.*, 26(28), 4820(2014).

28. S. Balendhran, S. Walia, H. Nili, S. Sriram and M. Bhaskaran, Elemental Analogues of Graphene: Silicene, Germanene, Stanene, and Phosphorene, *Small*, 11(6), 640(2015).

29. F. F. Zhu, W. J. Chen, Y. Xu, C. L. Gao, D. D. Guan, C. H. Liu, D. Qian, S. C. Zhang and J. F. Jia, Epitaxial growth of two-dimensional stanene, *Nat. Mater.*, 14(10), 1020(2015).

30. P. Z. Tang, P. C. Chen, W. D. Cao, H. Q. Huang, S. Cahangirov, L. D. Xian, Y. Xu, S. C. Zhang, W. H. Duan and A. Rubio, Stable Two-Dimensional Dumbbell Stanene: A Quantum Spin Hall Insulator, *Phys. Rev. B*, 90(12), 121408(2014).

31. S. Rachel and M. Ezawa, Giant Magnetoresistance and Perfect Spin Filter in Silicene, Germanene, and Stanene, *Phys. Rev. B*, 89(19), 195303(2014).

32. N. Gao, H. S. Liu, S. Zhou, Y. Z. Bai and J. J. Zhao, Interaction between Post-Graphene Group-IV Honeycomb Monolayers and Metal Substrates: Implication for Synthesis and Structure Control, *J. Phys. Chem. C*, 121(9), 5123(2017).

33. L. Li, Y. Yu, G. J. Ye, Q. Ge, X. Ou, H. Wu, D. Feng, X. H. Chen and Y. Zhang, Black Phosphorus Field-Effect Transistors, *Nat. Nanotech.*, 9(5), 372(2014).

34. H. O. Churchill and P. Jarillo-Herrero, Two-dimensional crystals: phosphorus joins the family, *Nat Nanotech.*, 9(5), 330(2014).

35. H. Liu, A. T. Neal, Z. Zhu, Z. Luo, X. Xu, D. Tománek, and P. D. Ye, Phosphorene: An Unexplored 2D Semiconductor with a High Hole Mobility, *ACS Nano*, 8 (4), 4033 (2014).

36. A. Carvalho, M. Wang, X. Zhu, A. S. Rodin, H. B. Su and A. H. C. Neto, Phosphorene: from theory to applications, *Nat. Rev. Mater.*, 1(11), 16061(2016).

37. Y. Jing, X. Zhang and Z. Zhou, Phosphorene: What can we know from computations? *Wiley Interdiscip. Rev.: Comput. Mol. Sci,* 6(1), 5(2016).

38. R. Fei and L. Yang, Strain-engineering the anisotropic electrical conductance of few-layer black phosphorus, *Nano Lett.*, 14(5), 2884(2014).

39. L. Wang, A. Kutana, X. Zou and B. I. Yakobson, Electro-mechanical anisotropy of phosphorene, *Nanoscale*, 7(21), 9746(2015).

40. H. S. Tsai, S. W. Wang, C. H. Hsiao, C. W. Chen, H. Ouyang, Y. L. Chueh, H. C. Kuo and J. H. Liang, Direct Synthesis and Practical Bandgap Estimation of Multilayer Arsenene Nanoribbons, *Chem. Mater.,* 28(2), 425(2016).

41. S. Zhang, Z. Yan, Y. Li, Z. Chen and H. Zeng, Atomically Thin Arsenene and Antimonene: Semimetal-Semiconductor and Indirect-Direct Band-Gap Transitions, *Angew. Chem. Int. Ed.*, 54(10), 3112(2015).

42. S. Zhang, S. Guo, Z. Chen, Y. Wang, H. Gao, J. Gómez-Herrero, P. Ares, F. Zamora, Z. Zhu and H. Zeng, Recent progress in 2D group-VA

semiconductors: From theory to experiment, *Chem. Soc. Rev.*, 47(3), 982(2018).

43. S. Zhang, M. Xie, F. Li, Z. Yan, Y. Li, E. Kan, W. Liu, Z. Chen and H. Zeng, Semiconducting Group 15 Monolayers: A Broad Range of Band Gaps and High Carrier Mobilities, *Angew. Chem. Int. Ed.*, 55(5), 1666(2016).

44. H. S. Tsai, C. W. Chen, C. H. Hsiao, H. Ouyang and J. H. Liang, The Advent of Multilayer Antimonene Nanoribbons with Room Temperature Orange Light Emission, *Chem. Commun.*, 52(54), 8409(2016).

45. P. Ares, F. Aguilar-Galindo, D. Rodriguez-San-Miguel, D. A. Aldave, S. Diaz-Tendero, M. Alcami, F. Martin, J. Gomez-Herrero and F. Zamora, Mechanical Isolation of Highly Stable Antimonene under Ambient Conditions, *Adv. Mater.,* 28(30), 6332(2016).

46. C. Gibaja, D. Rodriguez-San-Miguel, P. Ares, J. Gomez-Herrero, M. Varela, R. Gillen, J. Maultzsch, F. Hauke, A. Hirsch, G. Abellan and F. Zamora, Few-Layer Antimonene by Liquid-Phase Exfoliation*, Angew. Chem. Int. Ed.*, 55(46), 14345(2016).

47. J. Ji, X. Song, J. Liu, Z. Yan, C. Huo, S. Zhang, M. Su, L. Liao, W. Wang, Z. Ni, Y. Hao and H. Zeng, Two-Dimensional Antimonene Single Crystals Grown by Van Der Waals Epitaxy, *Nat. Commun.*, 7, 13352(2016).

48. J. H. Yuan, N. N. Yu, K. H. Xue and X. S. Miao, Stability, electronic and thermodynamic properties of aluminene from first-principles calculations, *Appl. Surf. Sci.*, 409, 85(2017).

49. C. Kamal, A. Chakrabarti and M. Ezawa, Aluminene as highly hole-doped graphene, *New J. Phys.*, 17(8), 083014(2015).

50. D. C. Tyte, $B^2[\pi]$-$A^2[\sigma]$) Band System of Aluminium Monoxide, *Nature*, 202(4930), 383(1964).

51. M. Hoch and H. L. Johnston, Formation, Stability and Crystal Structure of the Solid Aluminum Suboxides: Al_2O and AlO^1, *J. Am. Chem. Soc.*, 76(9), 2560(1954).

52. J. Koput and K. A. Peterson, Ab Initio Prediction of the Potential Energy Surface and Vibrational−Rotational Energy Levels of X^2A' BeOH, *J. Phys. Chem. A*, 107(19), 3981(2003).

53. C. Dohmeier, D. Loos and H. Schnockel, Aluminum(I) and gallium(I) compounds: Syntheses, structures, and reactions, *Angew. Chem. Int. Ed.,* 35(2), 129(1996).

54. C. Liang, Conduction characteristics of the lithium iodide-aluminum oxide solid electrolytes, *J. Electrochem. Soc.*, 120(10), 1289(1973).

55. S. Zhang, J. Yu, H. Li, D. Mao and G. Lu, High-effective approach from amino acid esters to chiral amino alcohols over $Cu/ZnO/Al_2O_3$ catalyst and its catalytic reaction mechanism, *Sci. Rep.*, 6, 33196(2016).

56. T. T. Song, M. Yang, J. W. Chai, M. Callsen, J. Zhou, T. Yang, Z. Zhang, J. S. Pan, D. Z. Chi, Y. P. Feng and S. J. Wang, The stability of aluminium oxide monolayer and its interface with two-dimensional materials, *Sci. Rep.*, 6, 29221(2016).

57. M. D. Segall, P. J. D. Lindan, M. J. Probert, C. J. Pickard, P. J. Hasnip, S. J. Clark and M. C. Payne, First-principles simulation: ideas, illustrations and the CASTEP code, *J. Phys. Condens. Mat.*, 14(11), 2717(2002).

58. M. Kuisma, J. Ojanen, J. Enkovaara and T. Rantala, Kohn-Sham potential with discontinuity for band gap materials, *Phys. Rev. B*, 82(11), 115106(2010).

59. I. E. Castelli, T. Olsen, S. Datta, D. D. Landis, S. Dahl, K. S. Thygesen and K. W. Jacobsen, Computational screening of perovskite metal oxides for optimal solar light capture, *Energy & Environ. Sci.*, 5(2), 5814(2012).

60. P. Miró, M. Ghorbani-Asl and T. Heine, Two Dimensional Materials Beyond MoS2: Noble-Transition-Metal Dichalcogenides, *Angew. Chem. Int. Ed.*, 53(11), 3015(2014).

61. H. Li, C. Tsai, A. L. Koh, L. Cai, A. W. Contryman, A. H. Fragapane, J. Zhao, H. S. Han, H. C. Manoharan and F. Abild-Pedersen, Activating and optimizing MoS 2 basal planes for hydrogen evolution through the formation of strained sulphur vacancies, *Nat. Mater.*, 15(1), 48(2016).

62. Y. Wang, J. Lv, L. Zhu and Y. Ma, Crystal structure prediction via particle-swarm optimization, *Phys. Rev. B*, 82(9), 094116(2010).

63. K. Takahashi, A. Yoshikawa and A. Sandhu, Wide bandgap semiconductors, *Springer-Verlag Berlin Heidelberg.*, 239(2007).

64. M. N. Yoder, *Electron Devices*, Wide bandgap semiconductor materials and devices, *IEEE T. Electron. Dev.,* 43(10), 1633(1996).

65. A. Lafond, C. Guillot-Deudon, J. Vidal, M. Paris, C. La and S. Jobic,

Substitution of Li for Cu in Cu_2ZnSnS_4: Toward Wide Band Gap Absorbers with Low Cation Disorder for Thin Film Solar Cells, *Inorg. Chem.*, 56(5), 2712(2017).

66. T. P. Chow and R. Tyagi, Wide bandgap compound semiconductors for superior high-voltage unipolar power devices, *IEEE T. Electron. Dev.*, 41(8), 1481(1994).

67. J. Casady and R. W. Johnson, Status of silicon carbide (SiC) as a wide-bandgap semiconductor for high-temperature applications, *Solid·State Electron*, 39(10), 1409(1996).

68. P. G. Neudeck, R. S. Okojie and L.-Y. Chen, High-temperature electronics-a role for wide bandgap semiconductors? *Proc. IEEE*, 90(6), 1065-1076(2002).

69. M. Topsakal, E. Aktürk and S. Ciraci, First-principles study of two-and one-dimensional honeycomb structures of boron nitride, *Phys. Rev. B*, 79(11), 115442(2009).

70. K. Watanabe, T. Taniguchi and H. Kanda, Direct-bandgap properties and evidence for ultraviolet lasing of hexagonal boron nitride single crystal, *Nat. Mater.*, 3(6), 404(2004).

71. Y. Kubota, K. Watanabe, O. Tsuda and T. Taniguchi, Deep ultraviolet light-emitting hexagonal boron nitride synthesized at atmospheric pressure, *Science*, 317(5840), 932(2007).

72. E. Monroy, F. Omnès and F. Calle, Wide-bandgap semiconductor ultraviolet photodetectors, *Semicond. Sci. Technol.*, 18(4), R33(2003).

73. H.-Y. Lu, A. S. Cuamba, L. Geng, L. Hao, Y.-M. Qi and C. Ting, C_3H_2: A wide-band-gap semiconductor with strong optical absorption, *Phys. Rev. B*, 96(16), 165420(2017).